Design of Glass Fibre Reinforced Polyester Monocoque for Formula Student Race Car

A. Olesen, C. Simonsen, J. Sørensen, N. Broberg, N. Radhakrishnan

Department of Materials and Production, Aalborg University
Fibigerstraede 16, DK-9220 Aalborg East, Denmark
Email: (amol15, csimon15, jbsa15, nbrobe15, nradha18)@student.aau.dk,
Web page: http://www.mechman.mp.aau.dk/

Abstract
This project deals with design of a glass fibre reinforced polyester monocoque for the AAU Racing team. The aim is to increase the torsional stiffness of the G8 chassis without increasing the total mass, whilst being compliant with the Formula Student rule set. In the design of the monocoque, focus is on manufacturability, attachment points, and best use of the geometry to increase torsional stiffness. To measure the forces acting on the suspension while driving, an experiment using strain gauges is conducted. An initial layup is made, which satisfies the Formula Student requirements regarding buckling modulus. To prevent failure, the layup is iteratively reinforced with respect to principal stresses and failure modes. Changing from the G8 space frame chassis to the hybrid monocoque results in an increase of 112% torsional stiffness, 9% mass, and 95% stiffness/mass ratio.

Keywords: Monocoque, FSAE, GFRP, sandwich structure, FEA, AAU Racing, Torsional Stiffness

1. Introduction

In race car design low mass and high stiffness are important features, particularly of the chassis. In general, three chassis designs exist — space frame, monocoque structure or a hybrid of the two. This paper focuses on the design of a hybrid fibre reinforced monocoque to replace the space frame chassis used by the Formula Student team AAU Racing on their G8 race car, and on increasing the torsional stiffness while maintaining mass, as this directly improves handling of the vehicle and simplifies the process of adjusting the suspension. The current G8 car is analysed wrt. torsional stiffness, vehicle components, and acting loads and relevant rules and requirements from [1] are presented.

1.1 G8 chassis and component overview

The G8 space frame chassis and attached components are shown on Fig. 1. The chassis primary structure consists of 7 parts, shown on Fig. 2. The rear structure is not considered in this paper, except its influence on overall stiffness and mounting points. The suspension, a double A-arm type with pull rod, also consists of 7 parts, see Fig. 3. The same suspension type is used on all wheels. The G8 suspension is used unchanged in the design of the monocoque.

1.2 Torsional stiffness

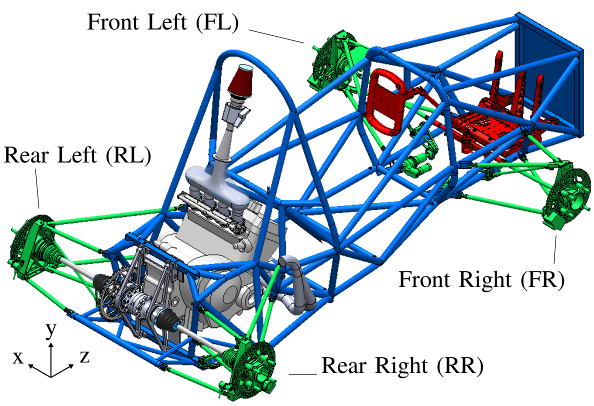

Fig. 1 AAU Racing G8 space frame chassis (blue), suspension system (green), steering and pedals (red) and power train (grey).

Per [2] the most significant effect of loads occurring at the wheels is a torsional moment along the length of the car, particularly during cornering (bending moments occur, but these are typically neglected). Under a given torque a stiffer chassis deforms less and stores less energy; steering is affected and becomes unpredictable when this energy is released, e.g. when exiting a corner, whereby stiffness is desirable. In [2] adequate torsional stiffness (measured as Nm/° between the axles) is estimated to be at least 3-5 times the roll stiffness (given by the suspension springs).

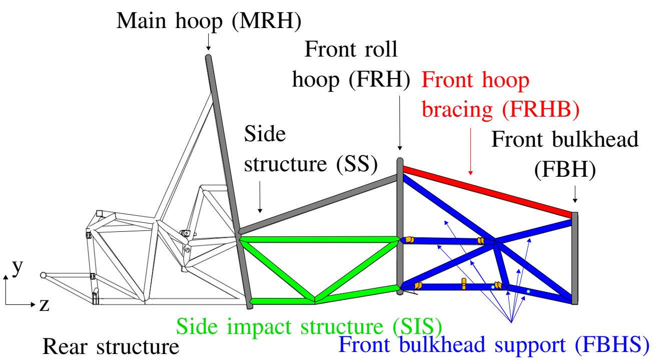

Fig. 2 Chassis terminology according to the Formula Student Germany (FSG) ruleset [1].

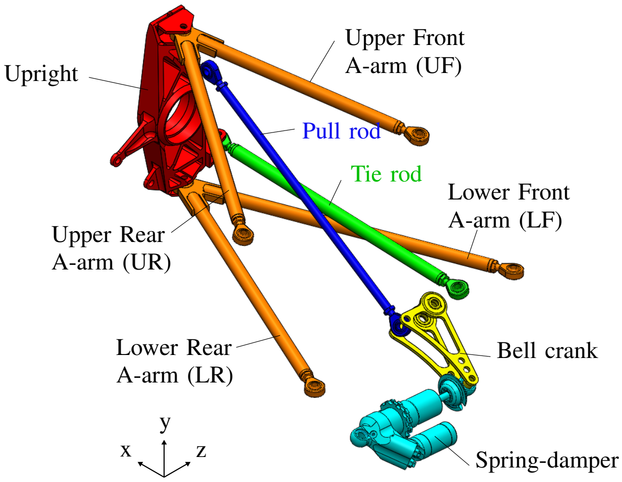

Fig. 3 FL suspension, as seen from drivers perspective.

1.2.1 Required torsional stiffness

Eq. 1 estimates the roll stiffness K_ϕ as the sum of front and rear stiffness, proposed by [3]:

$$K_\phi = \frac{\pi}{360^\circ}\left[\left(K_s\, t^2\, \eta_{IR}^2\right)_f + \left(K_s\, t^2\, \eta_{IR}^2\right)_r\right] \approx 490\ \mathrm{Nm}/^\circ, \tag{1}$$

where K_s is the spring stiffness of the spring-damper, t is the wheel track width, and η_{IR} is the ratio between spring and wheel travel, called installation ratio. The values used for the calculation are found in Tab. I. A minimum torsional stiffness of approximately 2500 Nm/° is required when using $5\,K_\phi$. [3] states that eq. 1 is only valid for cantilevered double A-arm, not a pull rod design like the G8's, but the results are used regardless as the difference in geometry is assumed negligible and the determined value is only a target.

1.2.2 G8 torsional stiffness and mass

	K_s [kN/m]	η_{IR} [-]	t [m]
Front	39	0.82	1.13
Rear	34	0.76	1.07

Tab. I Values for calculation of roll stiffness.

Via a CAD model of G8, mass of chassis, floor, and bodywork, which will be replaced by the monocoque, is found as 37.6 kg. A FE model of the G8 space frame using beam elements is made to determine torsional stiffness, with the rear suspension included as truss elements. Loads are applied at the front suspension pickup points as reactions to a remote load (force couple) located at the connection of upright and top A-arm, and the model is fixated in the same points on the rear uprights. The G8 torsional stiffness is determined as $1921.6\ \mathrm{Nm}/^\circ$.

1.3 Measurement of suspension forces

Suspension loads are directly measured on the G8 suspension during real driving. To simplify the experimental set-up and work required, all suspension members are assumed to be tension/compression bars only and that suspension loads are left/right symmetric for symmetric turns, such that only axial force is measured and only on the right side of the car.
To measure the loads, strain gauges (SG) are mounted on all suspension rods in the FR and RR suspensions. The SGs are installed in a half bridge configuration, such that bending is removed and only axial strain is measured [4]. The SGs are calibrated in a tension test up to 3 kN. During calibration it was found that the sensors (an Arduino Due and HX711 loadcells) drifted significantly. Drift was measured over a 64 hour period, with the largest drift being ≈7 N over 10 minutes, and a 10 minute interval between equipment zeroing was deemed appropriate.
Zeroing requires known loads; since removing all loads from the suspension during testing (i.e. disassembling the suspension entirely) would be too time-consuming, a static equilibrium of the suspension was calculated. With this the reaction forces in the suspension are found for wheels lifted entirely off the ground.

To help interpret the SG data, steering wheel position and suspension travel is measured simultaneously, such that the vehicle movements and behaviour are known.

1.3.1 Results

Due to limited time and testing facilities only one day was scheduled for testing. Unfortunately the G8 car had multiple issues on the day of testing; useful data were obtained only for 20 s of counter-clockwise (CCW) and 5 s of clockwise (CW) continuous cornering. The obtained data is however comparable with results from a previous generation car (G3) in a similar experiment [5], particularly when considering differences in chassis, suspension system, and driver. Large variations affect the measured suspension forces and thus the final force estimates presented in Tab. II are calculated by eq. 2

$$F_{final} = F \left(1 + \frac{1}{|F|}\, 3\sigma\right), \tag{2}$$

where F is measured force and σ is the attached standard deviation.

	FR suspension [N]		**RR suspension** [N]	
Position	**Inside**	**Outside**	**Inside**	**Outside**
UF	-1728	-1689	-917	-910
UR	3064	3617	-2355	1593
LF	2448	-1744	662	985
LR	2446	-3377	-3061	-4931
Tie rod	-1053	1138	894	-1360
Pull rod	2082	2806	2082	2805

Tab. II Final estimates of suspension loads during cornering.

1.4 Formula Student rules

All components on the car must comply with [1] to be used in competition. The chassis must be able to withstand loads as shown on Fig 5 and be spacious enough to accomodate templates for minimum cockpit opening and internal cross section, see Fig. 4. All chassis elements but the MRH and FRH may be laminated structures, however a maximum of 50 % of the fibres by mass may be within $\pm 10^{\circ}$ of each other. The FRH must be fully enclosed in fibres, as shown on Fig. 4. Finally structural equivalence to a baseline chassis must be proved.

1.4.1 Structural Equivalence Spreadsheet (SES)

The SES is an Excel spreadsheet prepared by competition officials in which the team enters dimensions and material properties of the primary structure. The SES is a safety measure where the buckling modulus (abbreviated as EI in [1]) and ultimate tensile strength (UTS) of the primary structure are compared to those of an equivalent steel space frame chassis. The EI is calculated with the second order moment of area (I) and one-ply equivalent stiffness of the laminate (E_{eq}) and the UTS is the product of failure strength and cross sectional area of the laminate used. For the SIS, an equivalent vertical (SIS V) and horizontal (SIS H) panel is determined. Core material stiffness and strength is not included in calculations. EI and UTS minimum values are listed in Tab. III.

Part	EI [kNm^2]	UTS [kN]
FBH	3.4	87.3
FBHS	4.0	99.9
FRHB	1.7	43.7
SIS V	3.4	131.0
SIS H	1.7	131.0

Tab. III Minimum EI and UTS of the primary structure.

For the competition each different sandwich structure has to be built as a representative panel and subjected to a three point bending test from where E_{eq} for each face sheet is calculated. However, in this project the E_{eq} is simulated using the ANSYS Composite PrepPost (ACP).

2. Design

The monocoque is considered as two parts — front (consisting of FBH, FBHS, FRHB, and FRH) and SIS. The method and location of attachment point is first decided, thereafter a design envelope for the front is made. The shape of the SIS is discussed and a final design shape for the monocoque is presented. The full design of the monocoque is seen on Fig. 7 and the entire car on Fig. 6.

2.1 Monocoque attachment points

The monocoque must support several components and their accompanying loads. The attachment points require careful design to avoid damaging the sandwich structure in normal use, particularly as most approximate point loads which are undesirable in general [6, 7]. The overall designs and locations of brackets and subframe used for attachments are seen on Fig. 7, and suspension points on Fig. 11. Methods and detailed designs are presented in the following.

2.1.1 FBHS bottom

Along the bottom of the front part, several components are attached: lower A-arms, bell cranks, spring-dampers, pedal box, and steering rack. As these components are in close proximity they are attached to a common steel tube on either side with bolted connections and the tube is locally reinforced with steel sleeve inserts; the spring-dampers are attached to the bottom of the FRH. The tubes are welded to the FRH and steering rack bridge, stiffening the structure, and the assembly is called the *subframe*. Beyond being a common attachment point, the subframe works to distribute the various point loads into the monocoque, reducing the magnitude of local effects. The brackets used to attach to the subframe are shown in Fig. 8. Subframe and brackets are designed for manufacture from standard tube dimension.

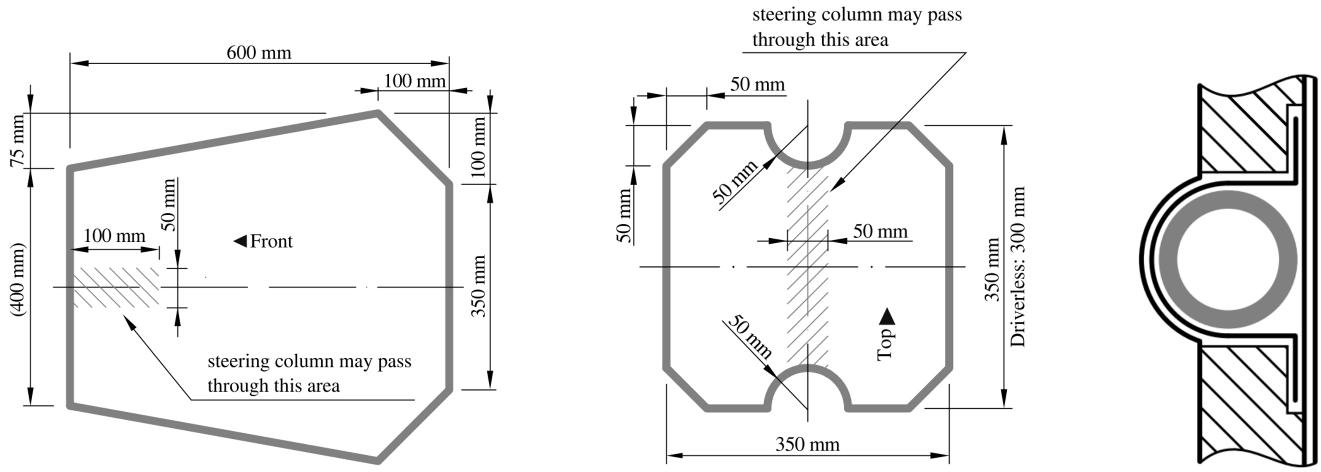

Fig. 4 *Left*: Cockpit opening template (COT). Must be accommodated between cockpit opening and a plane 320 mm above floor. *Center*: Cockpit internal template (CIT). Must be accommodated between FRH and a plane 100 mm from pedals (-100 mm along z-axis). *Right*: FRH fully encapsulated with fibres. All images from [1].

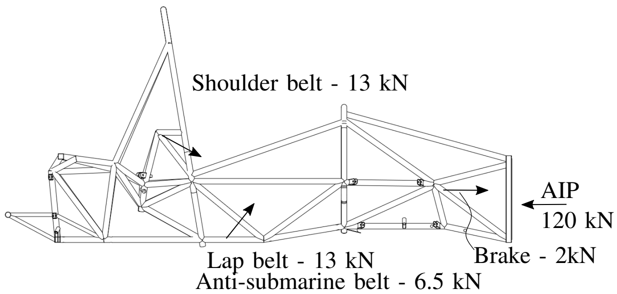

Fig. 5 Load requirements from [1]. The Anti Intrusion Plate (AIP) is attached across the FBH.

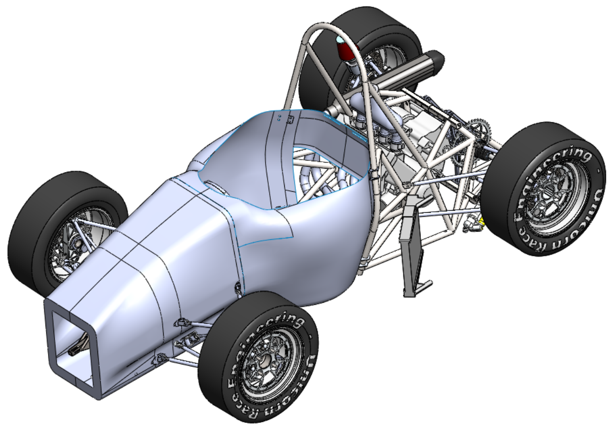

Fig. 6 Monocoque replacing G8 chassis.

2.1.2 Inserts and reinforcement

Inclusion of the subframe is inconvenient in several places (upper A-arms, MRH, belts) and inserts are used to attach directly to the monocoque instead. The insert is designed with reinforcement to reduce the risk of pullout, see Fig. 9 and two inserts to better transfer torque/remote loads. The numbering on Fig. 9 refers

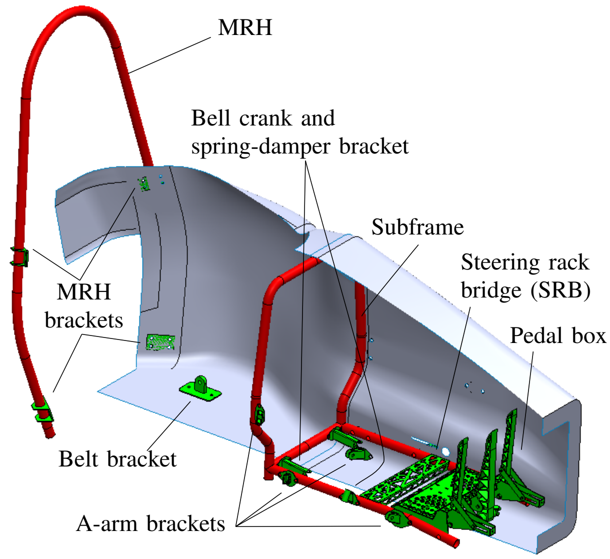

Fig. 7 Location of attachments (green), and subframe and MRH (red) in and on the monocoque.

to the assembly:

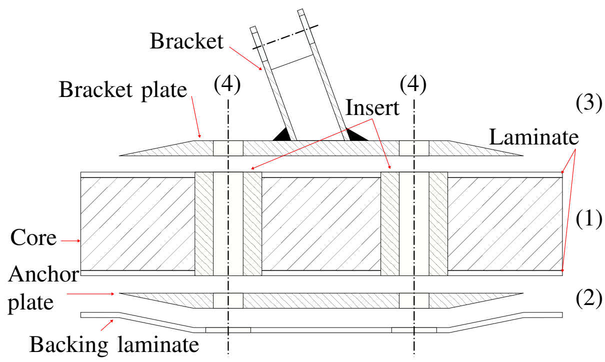

Fig. 9 Cross section of bracket, insert, and reinforcement.

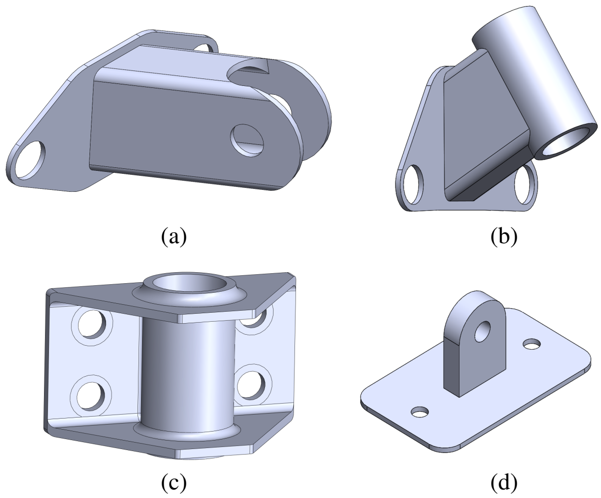

Fig. 8 Bracket designs: (a) A-arm and spring-damper, (b) bell crank, (c) MRH, with MRH tube shown installed, (d) seat belt.

(1) Sandwich structure and inserts are cast together via VARTM.
(2) Anchor plate is glued on and the backing laminate is overlaid as wet layup (simultaneous with wet layup of subframe and monocoque split lines).
(3) The outside bracket plate, with the bracket already welded onto it, is glued on.
(4) The whole assembly is bolted together.

Step (3) may be skipped, to allow adjustment of the bracket. Bracket plate is steel, such the bracket is more easily welded on and the inserts and anchor plate are aluminium. All metal components are sandblasted to improve glue bond.

2.1.3 Upper A-arms

As only two attachments per side are needed for the upper A-arms, the subframe is not designed to cover these points. Due to the fixed suspension positions, the front UR A-arm points are not moved rearwards to coincide with the FRH.

2.1.4 MRH

The brackets used for MRH connection is shown on Fig. 8. Per [1] at least four brackets are needed; top and bottom, left and right. The brackets are placed as close to the triangulation points between tubes in the rear structure as possible to reduce transfer of undesired bending loads.

2.1.5 Lap and anti-submarine belts

Lap and anti-submarine belts are attached in a common point on either side of the driver in the monocoque with a bracket as shown in Fig. 8.

2.1.6 FBH

On G8 the FBH is designed as smallest possible fit for the impact attenuator, and the FBH outer geometry is not changed for the monocoque. The inward geometry is a rectangular opening, as seen on Fig. 7. This design allows mounting the AIP with bolts onto inserts in the FBH. No reinforcement is made for the inserts — only small loads from the weight of the AIP act during normal operation and the 120 kN impact load acts parallel to fiber direction.

2.2 Front design envelope

Bracket positions and FBH define the outer limits of the design envelope and the CIT defines the inner, shown on Fig. 10 along with the final design of the front. On Fig. 11 the suspension attachment is shown with and without brackets.

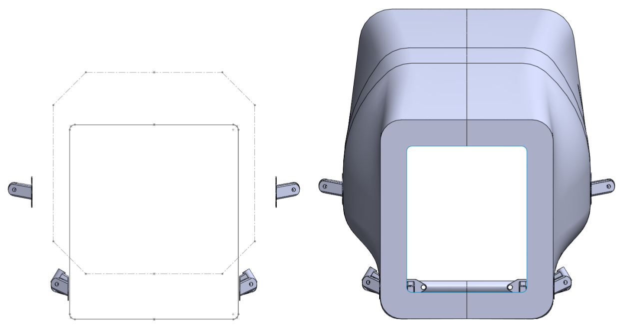

Fig. 10 Front design envelope. Full line is outer geometry of the FBH, dashed line is the CIT, off set by 25 mm, such there is room for building the sandwich structure inwards.

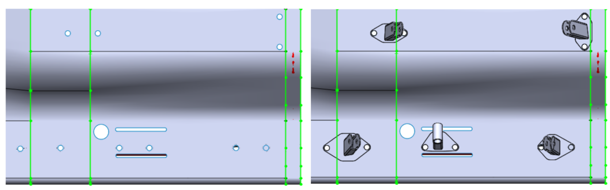

Fig. 11 Suspension attachment with and without brackets.

2.3 SIS

The SIS design envelope is constrained on the outside by FRH, MRH, and the track width of the car and on the inside by the MRH. The SIS is seen on Fig. 12.

2.3.1 Cockpit opening (CO)

To assist in determining the shape of the CO, three paper cylinders are made with a rectangular, an elliptical, and a COT-shaped hole in the side. These paper cylinders

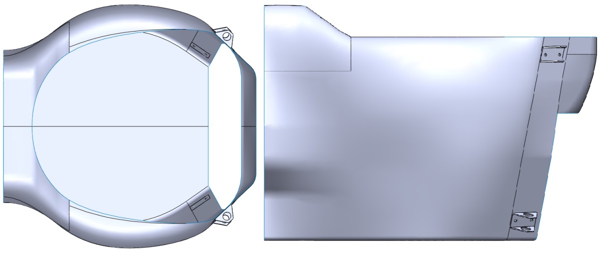

Fig. 12 SIS. left: Top view XZ plane. Right: Side view YZ-plane

are then subjected to a torque and their deformation behaviour is observed. The ellipse is the least compliant shape, likely because it has a smoother transition of stiffness, thus the CO is designed in this shape, while accommodating the COT.

2.3.2 Size

As the SIS design envelope is restrictive wrt. the width, torsional stiffness is increased by additional width, directly increasing the polar moment of inertia. Smooth surfaces with tangency and high curvature radius are desired to avoid abrupt stiffness changes and stress concentrations.

2.3.3 Rear opening

The opening in the monocoque at the MRH is made to accommodate engine components and electronics. In the current design the fuel tank is mounted below the driver, just in front of the opening, and fuel lines must pass rearwards to the engine. The same is true for engine start and emergency power off wires, and more if the engine control unit is placed inside the monocoque. The exhaust manifold occupies the space where the monocoque could be closed by flat surfaces, and to avoid manufacture of complicated geometry here, the hole is left open. The stiffness lost to this choice is not determined, but required stiffness is reached regardless. The opening later covered by a removable firewall (protection against hot components and fire hazards) and the driver seat.

3. Manufacturing considerations

Vacuum assisted resin transfer moulding (VARTM) is chosen for manufacturing, with hand layup of necessary details. VARTM is chosen as it is cheaper than pre-pregs and resin transfer moulding, while capable of relatively high fibre volume fractions (55% - 65%) [8]. [9] recommends to design a draft angle $> 3°$ and the mould is designed to be split into multiple sections to achieve a greater draft angle. It is recommended by [10] to use rounding radii larger than 3.175 mm to avoid dry spots, though [9] recommends 6.35 mm. The monocoque is likely to be manufactured by inexperienced workers, so the larger radius is chosen as minimum.

3.1 Manufacturing process

Manufacture begins with building a positive foam master plug, with flanges for mould split lines, see Fig. 13, and dowel pins for location of inserts. A glass fibre negative mould is cast on the master plug and around the details. The mould and monocoque are made in the same material, such that thermal expansion is the same and residual stresses are avoided in the finished monocoque. The monocoque is cast in two halves, split along the vertical symmetry plane, such the FRH and subframe insert can be included.

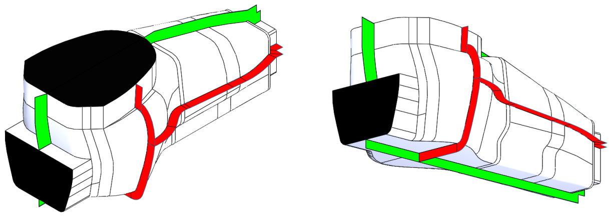

Fig. 13 Foam master plug. Green flanges are the monocoque split lines and are used to extend fibres onto during casting. Red flanges are split lines for the mould itself, to ease the de-moulding. Black faces are not used for the mould.

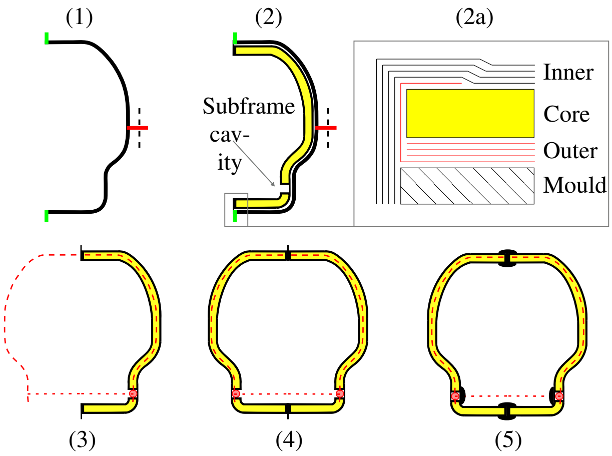

Fig. 14 Monocoque manufacturing process.

The casting process, shown on Fig. 14, is as follows:

(1) Glass fibre mould finished and ready for casting.
(2) Monocoque outer face, core, and inner face on the glass fibre mould, with subframe cavity.
(2a) Detailed view of monocoque edges. Fibres from outer face is used to make an end cap around the edge to prevent delamination. The inner fibres are laid onto the mould flange.

(3) Subframe is inserted in the cavity and fixed with a high viscosity adhesive on one side.
(4) The other side of the monocoque is made and fitted on the subframe following steps 1-3. The two sides are glued at the split lines.
(5) Fibre flanges are cut off. Wet layup of subframe and split line double lap joint. The fibres are laid in $\pm 45°$ and $90°$ to the covered lines, reinforcing the joint.

4. Material selection and layup

Traditionally monocoques are made from either glass fibre (GF) or carbon fibre (CF) reinforced plastics, with CF costing approximately 10 times more than GF [7]. Similarly common matrix materials are epoxy and polyester, where epoxy costs in the range of 4 times more than polyester. Due to Formula Student having a economics aspect, it is decided to use E-glass fibre reinforced polyester (GFRP). Raw material mechanical properties are shown in Tab. IV and V. Lamina mechanical properties are calculated by rule of mixture [6].

	GF	Polyester	
E	70	3.5	[GPa]
ν	0.22	0.37	[-]
ρ	2560	1200	[kg/m^3]

Tab. IV Material properties for GF and polyester [7].

	H80	H130	
E	90	170	[MPa]
G	27	50	[MPa]
ρ	80	130	[kg/m^3]

Tab. V Material properties core material [11].

4.1 Layup

As preliminary reflections of the layup, the paper cylinders are considered again. The deformation is mainly bending of the walls at the hole and torsion of the rest of the cylinder. Thus, layup targets are general torsional stiffness and SIS bending stiffness. Due to this fibres will primarily be orientated in $0°$ and $\pm 45°$ relative to the z-axis. On Fig. 15 the fibre orientation is classified. However, a SES-compliant layup needs many fibres in the lengthwise direction to increase the EI. The final layup after reinforcement needed for compliance with [1] is shown in Tab. VI.

5. Simulation

The simulation is split into three parts: loads required by [1], experimentally determined loads, and torsional stiffness. ACP is used for layup definitions and simulations are made in ANSYS Workbench. Only the laminated structure is simulated, without the subframe, due to uncertainty regarding connection between sub frame and laminate. The sub frame is assumed to make the monocoque stiffer, why it is assumed to be a fair assumption, disregarding the sub frame. SHELL281 elements are used because of better computational efficiency relative to SOLSH190 and better performance for curved structures relative to SHELL 181 [7].

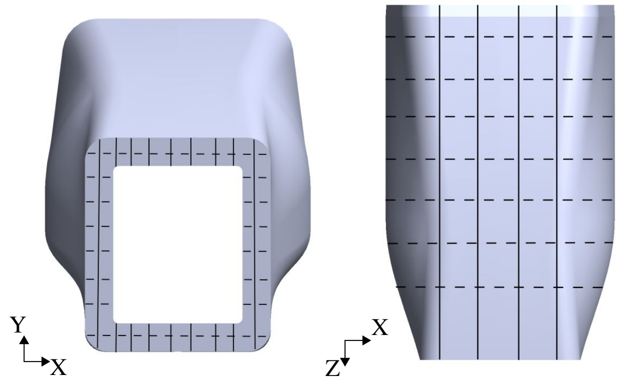

Fig. 15 Orientation of fibres. Full line is $0°$, dashed is $90°$.

5.1 Failure Criteria

Multiple failure criteria is applied — max stress, max strain, and Tsai-Wu criteria are applied for the face sheets and core failure for the core. Max stress and max strain are used to investigate failure modes and Tsai-Wu is used to account for stress interaction. For core failure ANSYS uses a simplified formulation of Tsai-Wu (Eq. 3), only including interlaminar shear stresses [12], for failure index

$$f = \left(\frac{\tau_{23}}{Q}\right)^2 + \left(\frac{\tau_{13}}{R}\right)^2, \tag{3}$$

Where Q and R are the shear failure stress in the 23 and 13 plane in the material coordinate, respectively. Due to uncertainty of fibre stress and strain limits, a failure index $f < 0.7$ is wanted in all criteria as a safety.

5.2 Formula Student loads

The AIP is required to withstand 120 kN [1], applied as a pressure on a steel plate at the front bulkhead. This lead to failure at the cockpit opening as seen on Fig. 16.

To define a new layup, failure modes and principal stresses are analysed, to better orient fibres in load directions. The new layup is shown in Tab. VI for the areas as shown in Fig. 17.

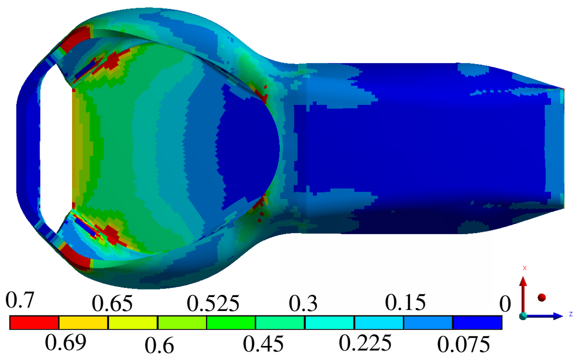

Fig. 16 Combined max failure index (all four criteria) for initial layup, subjected to a force of 120 kN at the front bulkhead. Core failure at top MRH connections and Tsai-Wu failure at front CO and bottom MRH connections.

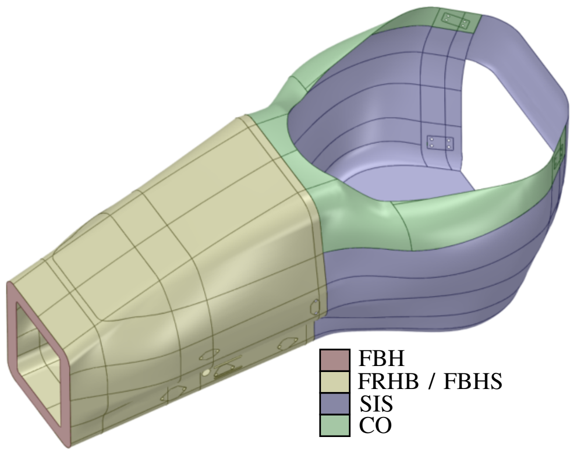

Fig. 17 Area definitions for the layup in Tab. VI.

The combined mass of monocoque, subframe and rear structure is 40.9 kg. Even with the new layup and a stiffer core, failure will occur in the CO at the MRH, due to the twist and proximity load application, Fig. 18. A redesign of this section is preferred to improve load path, instead of reinforcing the structure further.

5.3 Experimental loads

The insert reinforcement at the suspension is not implemented in the FE model and core failure is not considered. The monocoque does not fail due to the loads from the experiment, applied as distributed loads the shape of the bracket.

5.4 Torsional Stiffness

The simulation is done similarly as for the torsional stiffness of G8. The rear structure are simulated exactly as for G8. However the MRH and the MRH brackets are models as solids. The interaction between the MRH brackets and the monocoque are done using a bonded contact, where nodes on the surfaces in contact are restrained to have the same displacement. The torsional stiffness for the hybrid monocoque is $4070\mathrm{Nm}/^{\circ}$. The load application is shown on Fig. 19.

θ_{layer}	SIS	FRHB/ FBHS	FBH	CO	
$\pm45^{\circ}$	0.500	0.250	1.000	0.750	[mm]
90°	0.125	0.125	0.250	0.125	[mm]
0°	0.750	0.750	2.500	0.750	[mm]
90°	0.125	0.125	0.250	0.125	[mm]
$\pm45^{\circ}$	0.250	0.250	1.000	0.250	[mm]
Core	25.000	25.000	12.500	**30.000**	[mm]
$\pm45^{\circ}$	0.250	0.250	1.000	0.250	[mm]
90°	0.125	0.125	0.250	0.125	[mm]
0°	0.750	0.750	2.500	0.750	[mm]
90°	0.125	0.125	0.250	0.125	[mm]
$\pm45^{\circ}$	0.500	0.250	1.000	0.750	[mm]

Tab. VI New layup which comply with [1]. The CO core is the stiffer H130 foam instead of H80 used elsewhere. The layup satisfies the SES as well.

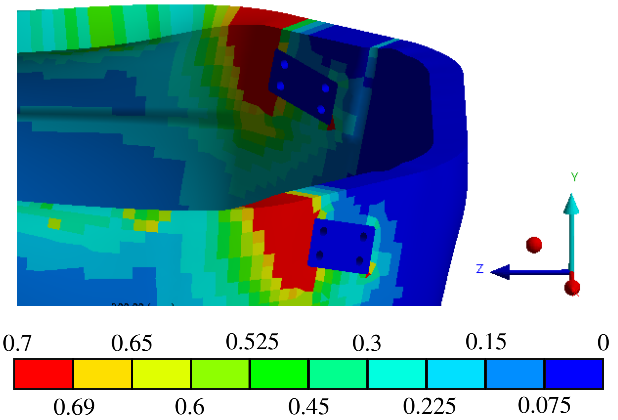

Fig. 18 Combined max failure index (all four criteria) for new layup, subjected to a force of 120 kN at the front bulkhead. Twist at rear of CO and core failure.

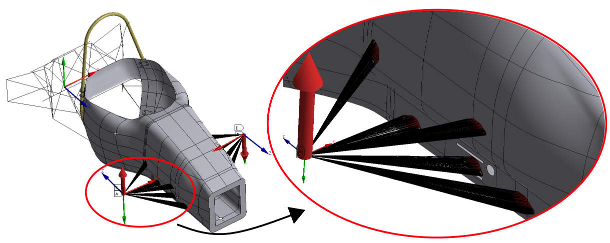

Fig. 19 Load application on the monocoque to determine torsional stiffness.

5.5 G8 vs hybrid monocoque

In eq. 4, it is shown that the torsional stiffness of the hybrid monocoque is 112 % larger than the stiffness of

G8.

$$\frac{4070\mathrm{Nm}/^\circ}{1920\mathrm{Nm}/^\circ} - 1 \approx 112\% \tag{4}$$

However, as it is seen in eq. 5 the mass is increased by 9 %

$$\frac{40.9\mathrm{kg}}{37.6\mathrm{kg}} - 1 \approx 9\% \tag{5}$$

Though, as it is shown in eq. 6 stiffness/mass ratio is increased by 95 %

$$\frac{\frac{4070\mathrm{Nm}/^\circ}{40.9\mathrm{kg}}}{\frac{1920\mathrm{Nm}/^\circ}{37.6\mathrm{kg}}} - 1 \approx \frac{99.5\mathrm{Nm}/^\circ/\mathrm{kg}}{51.1\mathrm{Nm}/^\circ/\mathrm{kg}} - 1 \approx 95\% \tag{6}$$

The hybrid monocoque does not accomplish the project aim. However, the benefits from increased stiffness vs the disadvantages from the increased mass are considered acceptable, due to the car should be far easier to steer, when exiting a corner — thus, cornering can be done at higher speed. Though, the increased mass decrease the braking and acceleration capabilities.

6. Further work

Further work is needed in regards to simulation, fatigue, and optimisation before the monocoque is ready for manufacture.

6.1 Simulation

To improve simulation accuracy the subframe should to be included, though it would require a full 3-D solid model. Similarly 3-D solid model are needed to simulate local effects of inserts and reinforcements.

6.2 Fatigue

Repeated loads (max. ≈ 5 kN from experiment) are small compared to the front impact load (120 kN) which is driving in the design. Thus, the static strength of the monocoque is likely large enough to avoid fatigue failure in the service life. Further, cracks are prone to grow from existing defects, thus time is better spent improving the manufacturing process, than attempting to simulate fatigue.

6.3 Optimisation

Several levels of optimisation are possible; as an expansion to the current design, the fibre orientation and layer thickness could be optimised to minimise mass. The optimisation should be constrained by:

- Max 50 % fibres within ±10°
- SES
- Min torsional stiffness of 1922 $\mathrm{Nm}/^\circ$
- Failure criteria for load cases: front impact, harness, braking, roll, and acceleration

Thickness and orientation should be discrete values given by single ply thickness and the simplification of possible layups, i.e. only 0°, ±45°, and 90°. The objective function (mass) is expected to be highly non-convex, as the stiffness (and thus mass required for stiffness constraint) varies sinusoidally with fibre orientation. Therefore, a non-deterministic optimisation algorithm is required to avoid convergence to local minima, such as Genetic Algorithm or Simulated Annealing [13]. Regardless of the optimisation scheme and extent of optimised variables, pre- and post-processing is required, e.g. ensuring manufacturable ply-drops and continuous layup between patches. A proposal for the optimisation scheme is shown on Fig. 20, ordered to improve computational efficiency (i.e. failing a design on least costly constraint calculations first).

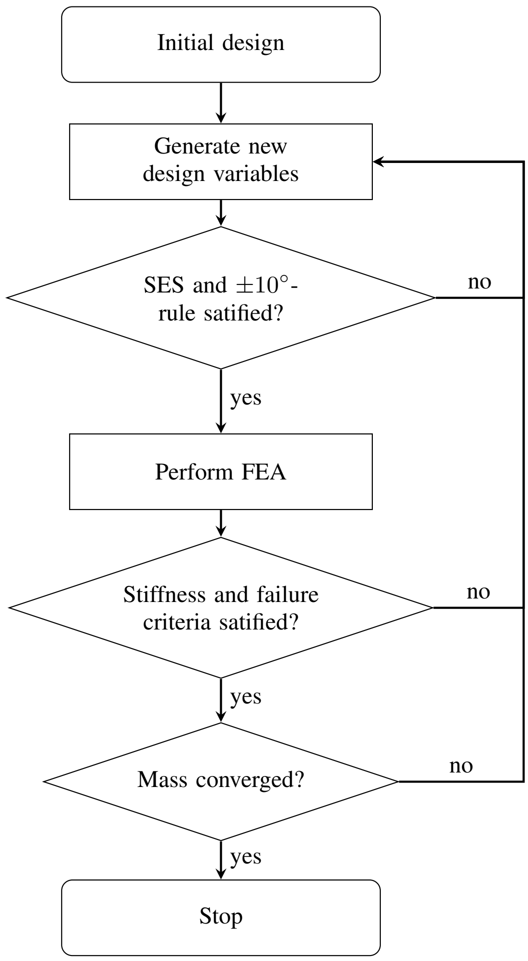

Fig. 20 Monocoque optimisation scheme.

7. Conclusion

A GFRP monocoque is designed to replace the AAU Racing G8 SIS, SS, FRH, FRHB, FBHS, and FBH. The monocoque has 112% higher torsional stiffness, 9% higher mass, and 95% higher stiffness/mass ratio than the G8 space frame. The monocoque satisfies all competition requirements, but has local core failure in the greatest load scenario (120 kN front impact), requiring more accurate simulations.

Acknowledgement

The authors of this work gratefully acknowledge Grundfos for sponsoring the 7th MechMan symposium and AAU Racing for providing useful CAD drawings of the G8 race car and for providing a base for acquiring data for the loads in the suspension system.

References

[1] FSG, Formula Student Germany Rules 2019 v1.1. https://www.formulastudent.de/fsg/rules/, 2018. Downloaded: 05-02-2019.

[2] W. F. Milliken and D. L. Milliken, "Race Car Vehicle Dynamics". No. ISBN: 1-56091-526-9, SAE, 1995.

[3] D. Seward, "Race Car Design". No. ISBN: 978-1-137-03014-6, Palgrave, 2014.

[4] K. Hoffmann, "An Introduction to Stress Analysis and Transducer Design using Strain Gauges". hbm.com, 2012.

[5] D. J. Meldgaard, E. Aldal, J. Vestergaard, M. Klith, R. Olesen, and S. B. Laustsen, "Design of a composite monocoque," 2009.

[6] R. M. Jones, "Mechanics of composites". No. ISBN: 978-1-56032-712-7 in 2nd edition, Taylor and Francis, 1999.

[7] E. Lund, "Mechanics of composite materials and structures," 2019. Downloaded: 27-2-2019.

[8] E. J. Barbero, "Introduction to Composite Materials Design". No. ISBN: 978-1-4398-9413-2 in 2nd edition, CRC Press, 2011.

[9] Molded Fiber Glass Companies, Technical Design Guide for FRP Composite Products and Parts. https://www.moldedfiberglass.com/sites/default/files/docs/MFG_Technical_Design_Guide_FRP_Composites_2018.pdf, 2018. Downloaded: 18-2-2019.

[10] S. Mazumdar, "Composites Manufacturing: Materials, Product, and Process Engineering". No. ISBN: 978-1-4200.4198-9 in 1st edition, CRC Press, 2002.

[11] D. Group, "Divinycell h technical data sheet," 2019.

[12] ANSYS, Core failure. https://www.sharcnet.ca/Software/Ansys/18.2.2/en-us/help/acp_ug/Core_Failure.html, 2017. Downloaded: 20-5-2019.

[13] J. S. Arora, Introduction to Optimum Design Fourth Edition. No. ISBN: 978-0-12-800806-5 in Elsevier Academic Press, Hardcover, Elsevier, 2016.